Analysis of Microwave Thawing of Slabs with Effective Heat Capacity Method

Tanmay Basak and K. G. Ayappa
Dept. of Chemical Engineering, Indian Institute of Science, Bangalore 560012, India

Microwave thawing of materials, which melt over a finite temperature range, are analyzed using the effective heat capacity method. The state of the material, solid, liquid or mush is deduced from the equilibrium liquid volume fraction vs. temperature relationship for the substance, and the microwave power is calculated from Maxwell's equations. Using Galerkin finite elements, the microwave power, temperature and liquid volume fractions were obtained for microwave thawing of tylose slabs. Thawing progresses from the inside and/or outside depending on the slab thickness. For slabs $\geq$ 5 cm, thawing progresses predominantly from the surface of the sample. Resonances, during which the microwave power absorption is high, causes the 2-cm slab to thaw quicker than 1-cm slabs. A power law for the thawing time vs. sample thickness yields an exponent of 1.56 for microwave thawing and 2 for conventional thawing. To control the temperature rise in the liquid regions, simulations were carried out with an on-off control on the microwave power. On-off control results in greater power savings for thick samples.

Introduction

Electromagnetic radiation in the frequency range 300 MHz to 300 GHz are known as microwaves. Microwave energy is used as a source of heat in applications such as heating, drying, sintering of ceramics, sterilization, thawing (melting) of food substances and frozen biological organs, and heating of emulsions. Datta (1990) reviews heat-and mass-transfer processes that occur during microwave heating of food. The ability of a material to heat when exposed to microwaves is dependent on the dielectric loss which reflects the capacity of the material to convert electrical energy to thermal energy. The spatially distributed absorbed microwave power is proportional to the frequency of radiation and the magnitude of the electric field in the sample. Frequencies commonly used for microwave heating are 300, 900 and 2,450 MHz. The domestic ovens operate at 2,450 MHz, and at this frequency the wavelength of radiation in the medium is typically a few cm.

Models for microwave heating of materials in the absence of a phase change formed the basis for a number of earlier studies (Ayappa et al., 1991, 1992; Chan et al., 1973; De Wagter, 1984; Jolly and Turner, 1990). In the above works, transient temperature profiles in objects exposed to plane waves are obtained by solving the appropriate energy balance equations with the microwave power derived from Maxwell's equations. Numerical and analytical techniques used to study microwave heating have been reviewed by Hill and Marchant (1996).

During thawing, a phase change occurs and models must predict the position of the phase change interface and total thawing times. Since foods are generally multicomponent in nature, thawing occurs over an extended temperature range, resulting in a heterogeneous region of coexisting solid and liquid phases commonly referred to as the "mushy" zone. Similar situations arise in solidification of alloys and metal casting. We will refer to techniques used to analyze the thawing of materials with a fixed melting point as *temperature methods* (Carslaw and Jaeger, 1959) and techniques for materials which melt over a range of temperatures as *enthalpy or effective heat capacity methods* (Dalhuijsen and Segal, 1986; Dantzig, 1989; Voller et al., 1990). The enthalpy and effective heat capacity methods are often referred to as fixed grid methods.

In the temperature method, energy balance equations for the liquid and solid phases are coupled with the Stefan or interface condition which involves the latent heat of melting and the velocity of the front. The temperature methods are most commonly used to analyze phase change in pure sub-

stances. In addition to being only an approximate formulation for materials that melt over a temperature range, the principal disadvantage of the temperature method is having to keep track of the moving phase change interface. This usually calls for an efficient moving mesh front tracking algorithm which can get quite cumbersome in the presence of multiple fronts. Nevertheless, a number of earlier works on microwave thawing were based on the temperature method.

Taoukis et al. (1987) used the isotherm migration method to analyze microwave thawing of frozen beef samples by assuming that the phase change occurs at a fixed melting point. Lambert's law, where the power decays exponentially into the sample, was used to describe the absorbed microwave power. When the average temperature in the frozen phase reached the melting point, the entire region was turned mushy and maintained at the melting point. The variation of the liquid volume fraction in the isothermal mushy zone was obtained by solving an additional energy balance equation. Pangrle et al. (1991) studied the thawing of frozen cylinders of water and NaCl using the temperature method with the microwave power derived from Maxwell's equations. The treatment of the mushy region was similar to that of Taoukis et al. (1987). For small NaCl cylinders, in addition to a front moving radially inward from the surface of the cylinder, thawing was also found to occur radially outward from the axis of the cylinder. Microwave thawing of multilayered slabs made up of ice and beef was studied by Pangrle et al. (1992). Slight superheating of the frozen region was observed in their study.

The enthalpy or effective heat capacity method is ideally suited to analyze thawing in materials that melt over a temperature range. Voller et al. (1990) reviews the extensive literature on the subject. The advantage of the effective heat capacity method is that a single energy balance equation is used for the entire domain, front tracking techniques are absent, and a fixed/uniform mesh is used. The latent heat is incorporated in the effective heat capacity and the local state of the material, solid, liquid, or mush is determined by the equilibrium liquid volume fraction vs. temperature relationship. In addition, numerical methods have been developed to use the effective heat capacity method for thawing of materials with a distinct melting point (Dalhuijsen and Segal, 1986; Dantzig, 1989). Due to the penetration of microwaves during microwave thawing of frozen foods, a phase change can occur at any given location in the sample. The effective heat capacity method is especially advantageous in these situations.

A few studies on microwave thawing with a Lambert's law formulation of the microwave power have been based on the effective heat capacity methods. Coleman (1990) while analyzing microwave thawing in a semi-infinite slab, observed superheating of the frozen region and subsequently used the enthalpy formulation to overcome this problem. Zeng and Faghri (1994) analyzed the thawing of tylose (23% methyl cellulose gel) using the effective heat capacity method and a Lambert's law formulation of the absorbed microwave power. Using a 2-D model, they found that the temperatures predicted by the model at the end of thawing were lower than that observed experimentally. This could be due partly to the Lambert's law representation of the absorbed power.

Here, we carry out a detailed analysis of microwave thawing using the effective heat capacity method for slabs exposed to uniform plane waves at 2,450 MHz. The energy balance equation is solved along with the Maxwell's equations using the Galerkin finite-element method to obtain the absorbed microwave power, temperature, and liquid volume fraction profiles for various slab thicknesses. Simulations are carried out for tylose whose dielectric and thermal properties mimic those of frozen meats. One of the practical problems encountered during microwave heating is the overheating of liquid regions which have a higher dielectric loss when compared with the frozen or mushy regions. This leads to hot spots and a wasteful expenditure of power. To control the temperature rise in the liquid regions during microwave thawing, simulations are carried out with an on-off control on the microwave power.

Theory

Effective heat capacity formulation

Consider a partially thawed sample as shown in Figure 1. Here, the material being thawed consists of a solid, liquid and mushy zone with the temperatures in the mushy zone spanning the range over which the phase change occurs. In the enthalpy formulation the domain is governed by a single energy balance equation

$$\frac{\partial H}{\partial t} = \nabla \cdot k_{\text{eff}} \nabla T + p(T), \tag{1}$$

The expression for the specific enthalpy, H ($\text{J} \cdot \text{m}^{-3}$) which is a function of the temperature at a given location in the sample, is (Dalhuijsen and Segal, 1986)

$$H(T) = (1-\phi_l)\int_{T_0}^{T} \rho C_s(\alpha)\, d\alpha + \phi_l \left[\int_{T_0}^{T_i} \rho C_s(\alpha) + \rho\lambda + \int_{T_i}^{T} \rho C_l(\alpha)\, d\alpha \right], \tag{2}$$

where C_l and C_s are the heat capacities ($\text{J} \cdot \text{kg}^{-1} \cdot \text{K}^{-1}$) of the liquid and solid phases respectively, T_0 is a reference temperature, T_i the initial melting point is the temperature at which the first drop of liquid forms, and ϕ_l the liquid volume

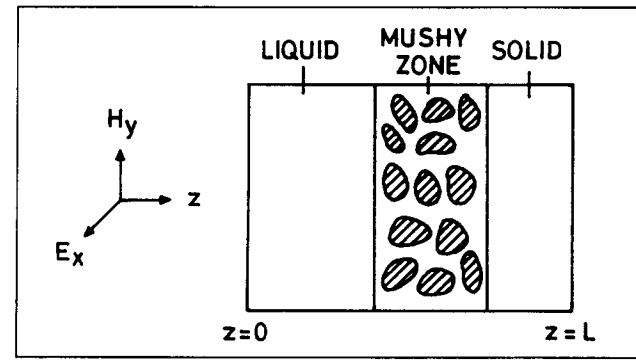

Figure 1. Liquid, solid and mushy regions in a partially thawed sample.

For a given temperature profile, the liquid volume fraction ϕ_l is determined from the ϕ_l vs. T relationship for the material.

fraction is a function of the temperature at a given point in the sample. The details of the variation of ϕ_l with T depends on the material being thawed. In Eq. 1 the effective thermal conductivity $k_{\text{eff}} = \phi_l k_l + (1-\phi_l)k_s$, where k_l and k_s are the thermal conductivities ($\text{W}\cdot\text{m}^{-1}\cdot\text{K}^{-1}$) of the liquid and solid phases, respectively, and $p(T)$ ($\text{W}\cdot\text{m}^{-3}$) is the absorbed microwave power is proportional to the electric field intensity in the sample and the frequency dependent dielectric loss. Neglecting buoyancy effects, ρ in Eq. 2 represents a mean density between the two phases.

In the effective heat capacity method the energy balance, Eq. 1, is reduced to an equation involving a single dependent variable T

$$C_{\text{eff}}\frac{\partial T}{\partial t} = \nabla\cdot k_{\text{eff}}\nabla T + p(T), \tag{3}$$

where the effective heat capacity

$$\begin{aligned} C_{\text{eff}} &= dH/dT \\ &= \frac{d\phi_l}{dT}\left[\rho C_s(T_i - T) + \rho\lambda + \rho C_l(T - T_i)\right] \\ &\quad + (1-\phi_l)\rho C_s + \phi_l \rho C_l. \end{aligned} \tag{4}$$

Discontinuities can occur in C_{eff} depending on the functional form of ϕ_l vs T.

We consider the microwave thawing in a slab of thickness $2L$ exposed to uniform plane waves as shown in Figure 2. Initially, the sample is completely frozen at a uniform temperature T_0. The thermal properties in the slab are assumed to be isotropic and the surrounding medium is at the ambient temperature T_∞ during the entire thawing period. At the sample boundaries heat is lost by convection. Using the following dimensionless variables,

$$z = \frac{Z+L}{2L},\quad \theta = \frac{T-T_\infty}{T_0},\quad Bi = \frac{2hL}{k} \quad \text{and} \quad \tau = \frac{\alpha_0 t}{4L^2}. \tag{5}$$

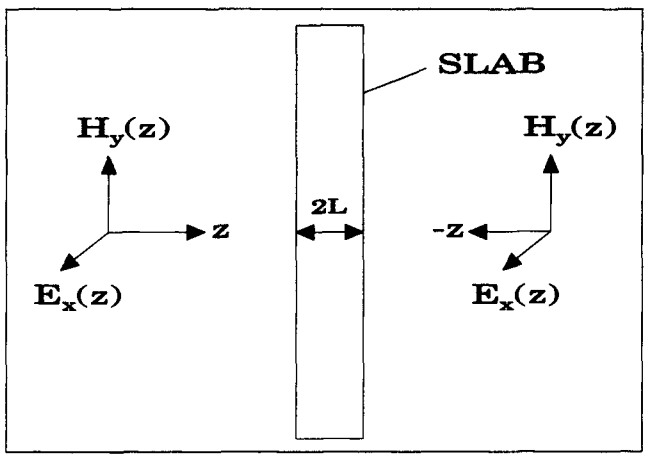

Figure 2. Slab exposed to plane electromagnetic waves at normal incidence.

where $-L \le z \le L$, h is the heat-transfer coefficient ($\text{W}\cdot\text{m}^{-2}\cdot\text{k}^{-1}$), Bi is the Biot number, and α_0 is a reference diffusivity ($\text{m}^2\cdot\text{s}^{-1}$).

Equation 3 for a 1D slab is

$$\bar{C}_{\text{eff}}\frac{\partial\theta}{\partial\tau} = \frac{\partial}{\partial z}\left(\bar{k}_{\text{eff}}\frac{\partial\theta}{\partial z}\right) + P(\theta), \tag{6}$$

where

$$P = \frac{4pL^2}{k_0 T_0},\quad \bar{C}_{\text{eff}} = \frac{C_{\text{eff}}}{\rho_0 C_{p,0}} \quad \text{and} \quad \bar{k}_{\text{eff}} = \frac{k_{\text{eff}}}{k_0}.$$

where P is the dimensionless microwave source term. Here ρ_0, $C_{p,0}$ and k_0 are the reference density, heat capacity, and thermal conductivity, respectively. The initial condition is

$$\theta(\tau = 0) = \frac{T_0 - T_\infty}{T_0} \quad \text{for} \quad 0 \le z \le 1, \tag{7}$$

and the boundary conditions are

$$\frac{\partial\theta}{\partial z} - Bi\,\theta = 0 \quad \text{at} \quad z = 0,$$

and

$$\frac{\partial\theta}{\partial z} + Bi\,\theta = 0 \quad \text{at} \quad z = 1. \tag{8}$$

The temperature-dependent microwave power term in Eq. 6 is obtained by solving the electric field equations simultaneously with Eq. 6.

Electric field equations for a slab

Microwaves are assumed to be incident normally on the opposite faces of the slab as shown in Figure 2. For propagation of uniform plane waves, the electric and magnetic components lie in a plane $(x-y)$ of uniform intensity and vary only in the direction of propagation (z-axis). The equation for the electric field E_x ($\text{V}\cdot\text{m}^{-1}$) in the slab (see Appendix) is

$$\frac{d^2E_x}{dZ^2} + k^2(\phi_l)\,E_x = 0, \tag{9}$$

where ϕ_l is the liquid volume fraction and $k = \omega\sqrt{\kappa'(\phi_l) + i\kappa''(\phi_l)}/c$ is the spatially varying propagation constant dependent on $\kappa'(\phi_l)$ the relative dielectric constant, and $\kappa''(\phi_l)$ the relative dielectric loss. Here, $\omega = 2\pi f$, where f is the frequency (Hz) of the electromagnetic radiation and c is the velocity of light ($\text{m}\cdot\text{s}^{-1}$). We assume that the dielectric properties are functions of temperature only due to their dependence on ϕ_l. Hence, in regions of pure liquid and solid,

the dielectric properties are assumed to be independent of temperature. Previous studies on the influence of temperature-dependent dielectric properties indicate that this is a good assumption at 2,450 MHz (Ayappa et al., 1991).

The expression for the relative complex dielectric constant $\kappa^* = \kappa' + i\kappa''$ in the mushy zone, based on Fricke's (1955) complex conductivity model is

$$\kappa^* = \frac{\kappa_c^*[\kappa_d^*(1+s_dV_d)+\kappa_c^*(1-V_d)s_d]}{[\kappa_c^*(s_d+V_d)+\kappa_d^*(1-V_d)]}, \qquad (10)$$

where κ_c^* and κ_d^* are the relative complex dielectric properties of the continuous and dispersed phases respectively, $s_d = 2$ for spherical dispersions, and $s_d = 1$ for cylindrical dispersions. V_d the volume fraction of the dispersed phase is $1-\phi_l$, when the solid is the dispersed phase (liquid continuous), and $V_d = \phi_l$, when liquid is the dispersed phase (solid continuous).

The wavelength λ_m and penetration depth D_p within a sample for a radiation of frequency f are related to κ' and κ'' as follows

$$\lambda_m = \frac{c}{f}\left(\frac{\kappa'\left(\sqrt{1+\left(\frac{\kappa''}{\kappa'}\right)^2}+1\right)}{2}\right)^{-1/2}, \qquad (11)$$

and

$$D_p = \frac{c}{2\pi f}\left(\frac{\kappa'\left(\sqrt{1+\left(\frac{\kappa''}{\kappa'}\right)^2}-1\right)}{2}\right)^{-1/2}. \qquad (12)$$

D_p is defined as the distance at which the field intensity decreases to $1/e$ of its incident value.

The power absorbed per unit volume is

$$p = \frac{1}{2}\omega\epsilon_0\kappa''E_x^2, \qquad (13)$$

where ϵ_0 is the free space permittivity (Farad$\cdot$m^{-1}) and the relationship between the flux of incident radiation I_0 in free space to the electric field intensity E_x is

$$I_0 = \frac{1}{2}c\epsilon_0E_x^2. \qquad (14)$$

For a slab exposed to radiation of intensity E_L from the left and E_R from the right, as shown in Figure 2, the radiation boundary conditions (Ayappa et al., 1991) are

$$\frac{dE_x}{dZ}+\frac{i\omega E_x}{c} = \frac{2i\omega}{c}E_Le^{-i\omega L/c} \quad \text{at} \quad Z=-L,$$
$$\frac{dE_x}{dZ}-\frac{i\omega E_x}{c} = -\frac{2i\omega}{c}E_Re^{-i\omega L/c} \quad \text{at} \quad Z=L. \qquad (15)$$

It is assumed in the model that the liquid and solid phases are always separated by a mushy region (Figure 1) which is found to be true for all the cases simulated here. This coupled with the continuity of the ϕ_l vs. T relationship always ensures that the dielectric properties are continuous across the slab. Hence, interface conditions between solid and mush or liquid and mush are not required while solving the electric field equation.

Using the dimensionless variables

$$u_x = \frac{E_x}{E_L} \quad \text{and} \quad z = \frac{Z+L}{2L},$$

Equation 9 reduces to

$$\frac{d^2u_x}{dz^2}+\gamma^2(\phi_l)u_x = 0, \qquad (16)$$

where u_x is the electric field intensity and $\gamma(\phi_l) = 2L\omega\sqrt{\kappa'(\phi_l)+i\kappa''(\phi_l)}/c$ is the propagation constant.

Solution procedure

The energy balance equation Eq. 6 and the field equation Eq. 16 are solved using the Galerkin finite-element method. Except for the time integration scheme, the solution procedure follows from an earlier work where we studied the heating of materials with temperature-dependent dielectric and thermal properties (Ayappa et al., 1991). For completeness, the method is only briefly outlined here. Substituting the complex field variable $u_x = v_x + iw_x$, into Eq. 16 and equating the real and imaginary components

$$\frac{d^2v_x}{dz^2}+\psi(\phi_l)v_x-\chi(\phi_l)w_x = 0 \qquad (17)$$

and

$$\frac{d^2w_x}{dz^2}+\chi(\phi_l)v_x+\psi(\phi_l)w_x = 0, \qquad (18)$$

where $\psi(\phi_l) = \frac{4L^2\omega^2}{c^2}\kappa'(\phi_l)$ and $\chi(\phi_l) = \frac{4L^2\omega^2}{c^2}\kappa''(\phi_l)$.

The boundary conditions for the real and imaginary components from Eqs. 15 are

$$\left.\begin{aligned}\frac{dv_x}{dz}-\frac{2\omega L}{c}w_x &= \frac{4\omega L}{c}\sin\left(\frac{\omega L}{c}\right)\\ \frac{dw_x}{dz}+\frac{2\omega L}{c}v_x &= \frac{4\omega L}{c}\cos\left(\frac{\omega L}{c}\right)\end{aligned}\right\} \quad \text{at} \quad z=0 \qquad (19)$$

and

$$\left.\begin{aligned}\frac{dv_x}{dz}+\frac{2\omega L}{c}w_x&=-\frac{E_R}{E_L}\frac{4\omega L}{c}\sin\left(\frac{\omega L}{c}\right)\\ \frac{dw_x}{dz}-\frac{2\omega L}{c}v_x&=-\frac{E_R}{E_L}\frac{4\omega L}{c}\cos\left(\frac{\omega L}{c}\right)\end{aligned}\right\}\quad\text{at}\quad z=1. \tag{20}$$

The expression for the microwave power term in Eq. 6 is

$$P[\phi_l(\theta)]=\frac{2L^2\omega\epsilon_0\kappa''(\phi_l)E_L^2}{k_0T_0}(v_x^2+w_x^2). \tag{21}$$

The Galerkin finite-element method is used to solve the coupled nonlinear equations Eqs. 6, 17, and 18. Expanding the real (v_x) and imaginary components (w_x) of the electric field, and the temperature (θ) in a basis set $\{\phi\}$

$$v_x\approx\sum_{k=1}^{N}v_k\phi_k(z),\quad w_x\approx\sum_{k=1}^{N}w_k\phi_k(z)$$

and

$$\theta\approx\sum_{k=1}^{N}\theta_k(\tau)\phi_k(z) \tag{22}$$

for

$$0\le z\le 1,$$

the Galerkin finite-element method yields the following nonlinear residual equations for Eqs. 6, 17 and 18, respectively.

$$\begin{aligned}R_i^{(1)}=&\sum_{k=1}^{N}v_k^{t+1}\int_0^1\phi_i'\phi_k'dz-\sum_{k=1}^{N}v_k^{t+1}\int_0^1\psi(\phi_l^{t+1})\phi_i\phi_k dz\\&+\sum_{k=1}^{N}w_k^{t+1}\int_0^1\chi(\phi_l^{t+1})\phi_i\phi_k dz+\frac{2\omega l}{c}w_1^{t+1}\delta_{i1}\\&+\frac{4\omega L}{c}\sin(\omega L/c)\delta_{i1}+\frac{2\omega L}{c}w_N^{t+1}\delta_{iN}\\&+\frac{E_R}{E_L}\frac{4\omega L}{c}\sin(\omega L/c)\delta_{iN},\end{aligned} \tag{23}$$

$$\begin{aligned}R_i^{(2)}=&\sum_{k=1}^{N}w_k^{t+1}\int_0^1\phi_i'\phi_k'dz-\sum_{k=1}^{N}v_k^{t+1}\int_0^1\chi(\phi_l^{t+1})\phi_i\phi_k dz\\&-\sum_{k=1}^{N}w_k^{t+1}\int_0^1\psi(\phi_l^{t+1})\phi_i\phi_k dz-\frac{2\omega L}{c}v_1^{t+1}\delta_{i1}\\&+\frac{4\omega L}{c}\cos(\omega L/c)\delta_{i1}-\frac{2\omega L}{c}v_N^{t+1}\delta_{iN}\\&+\frac{E_R}{E_L}\frac{4\omega L}{c}\cos(\omega L/c)\delta_{iN},\end{aligned} \tag{24}$$

$$\begin{aligned}R_i^{(3)}=&\sum_{k=1}^{N}\int_0^1[\bar{C}_{\text{eff}}(\phi_l^{t+1},\theta^{t+1})]\left\{\frac{\theta_k^{t+1}-\theta_k^t}{\Delta\tau}\right\}\phi_i\phi_k dz\\&+\frac{1}{2}[F(\theta^{t+1},v^{t+1},w^{t+1},\phi_l^{t+1})+F(\theta^t,v^t,w^t,\phi_l^t)]\end{aligned} \tag{25}$$

where

$$\begin{aligned}F(\theta^t,v^t,w^t,\phi_l^t)=&\sum_{k=1}^{N}\theta_k^t\int_0^1\bar{k}_{\text{eff}}(\phi_l^t)\phi_i'\phi_k'dz-\frac{2L^2\omega\epsilon_0E_L^2}{k_0T_0}\\&\times\int_0^1\kappa''(\phi_l^t)\left\{\left(\sum_k v_k^t\phi_k\right)^2+\left(\sum_k w_k^t\phi_k\right)^2\right\}\phi_i dz\\&+\bar{k}_{\text{eff},1}(\phi_l^t)Bi_1(\phi_l^t)\theta_1^t\delta_{i1}+\bar{k}_{\text{eff},N}(\phi_l^t)Bi_N(\phi_l^t)\theta_N^t\delta_{iN},\end{aligned} \tag{26}$$

and

$$i=1\ \ldots\ N\quad\text{and}\quad t=\text{time index}$$

The Crank-Nicholson method, which is an unconditionally stable algorithm, is used to discretize the time domain, and quadratic basis functions with three point Gaussian quadrature is used to evaluate the integrals in the residual equations. The nonlinear residual equations (Eqs. 23, 24 and 25) are solved using a Newton-Raphson procedure to determine the coefficients of the expansions in Eq. 22 at each time step. At each time step, the linear ($3N\times 3N$) system solved is

$$\boldsymbol{J}(\boldsymbol{u}^{n,t+1})[\boldsymbol{u}^{n,t+1}-\boldsymbol{u}^{n+1,t+1}]=\boldsymbol{R}(\boldsymbol{u}^{n,t+1}), \tag{27}$$

where n is the Newton iterate index and t the time index (s). The elements of the Jacobian matrix, $\boldsymbol{J}(\boldsymbol{u}^{n,t+1})$ contains the derivatives of the residual equations with respect to the temperature (θ_k's) and electric field unknowns (v_k's and w_k's) and $\boldsymbol{R}(\boldsymbol{u}^{n,t+1})$ is the vector of residuals.

Results and Discussion

Material properties and numerical tests

The microwave thawing process is examined for the material tylose. Thermal and dielectric data at 2,450 MHz for both the solid and liquid phases of tylose are given in Table 1. It is worth mentioning that the dielectric and thermal data for tylose mimic those of lean beef and is used as a substitute for frozen beef while carrying out microwave related experiments (Taoukis et al., 1987; Zeng and Faghri, 1994). We have neglected buoyancy effects and assumed a constant value of 1,000 $\text{kg}\cdot\text{m}^{-3}$ for the density of both the liquid and solid phases of tylose. The material properties in the mushy region

Table 1. Thermal and Dielectric Properties for Water and Tylose in Solid (s) and Liquid (l) phases (Taoukis et al., 1987)

Material	Water_s	Water_l	Tylose_s	Tylose_l
Heat capacity, $C_p[\text{J}\cdot\text{kg}^{-1}\cdot\text{k}^{-1}]$	2,051	4,226	2,090	3,520
Thermal conductivity, $k[\text{W}\cdot\text{m}^{-1}\cdot\text{k}^{-1}]$	2.22	0.56	1.3	0.5
Density, $\rho[\text{kg}\cdot\text{m}^{-3}]$	917	999	961	1,057
Latent heat, $\lambda[\text{J}\cdot\text{kg}^{-1}]$	3.34×10^5		2.34×10^5	
Dielectric constant (2,450 MHz), κ'	3.95	78.0	6.0	50.0
Dielectric loss (2,450 MHz), κ''	0.3	12.48	1.5	17.0

are functions of the liquid volume fraction ϕ_l, which is in turn a function of the temperature T. The functional form of ϕ_l vs. T for tylose is similar to that used by Zeng and Faghri (1994)

$$\phi_l = \begin{cases} 0 & T < T_i \\ \dfrac{(T-T_i)^2}{(T_f-T_i)(T_m-T_i)} & T_i \le T \le T_m \\ 1-\dfrac{(T-T_f)^2}{(T_f-T_i)(T_f-T_m)} & T_m \le T \le T_f \\ 1 & T > T_f, \end{cases} \tag{28}$$

where T_m is the temperature at which the latent heat release is a maximum and T_f is the final thawing temperature. The parameter values for T_i, T_m and T_f, in Eq. 28 are 265 K, 270 K, and 272.4 K respectively. Figure 3a illustrates the dependence of ϕ_l with T and Figure 3b illustrates the dependence of the effective heat capacity, C_{eff} (Eq. 4) with T. Note that the particular functional form of Eq. 28 yields a continuous $C_{\text{eff}}(T)$ function.

The effective dielectric constants in the mushy zone depend on whether the solid or liquid forms the continuous phase. In previous microwave heating simulations (Taoukis et al., 1987; Pangrle et al., 1991) effective dielectric properties in the mushy region were calculated by assuming that the solid forms the continuous phase. If this is true during the initial stages of thawing, the microstructure must change to one where the liquid forms the continuous phase towards the final stages of thawing. This issue has received little attention in the literature. Since melting is initiated at the grain boundaries of the solid phase, the microstructure of the mushy zone is typically characterized by a solid dispersed in a continuous liquid phase. In the present study, we evaluate the dielectric properties by assuming that the liquid forms the continuous phase in the mushy zone. We also carry out a few simulations to contrast the differences in thawing with the dielectric properties evaluated by assuming a solid continuous mushy zone. Figure 4 illustrates the variation of κ' and κ'' with the liquid volume fraction ϕ_l for both the liquid continuous (LC) and solid continuous (SC) mushy zones. All our calculations

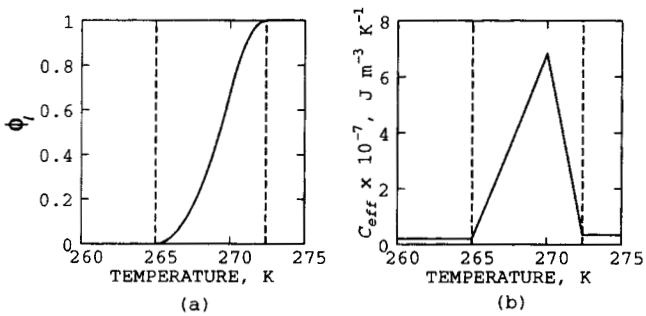

Figure 3. Variation of (a) liquid volume fraction, ϕ_l (Eq. 28); (b) effective heat capacity C_{eff} (Eq. 4) with temperature for tylose.

The continuity in the effective heat capacity function is due to the particular functional form of $\phi_l(T)$.

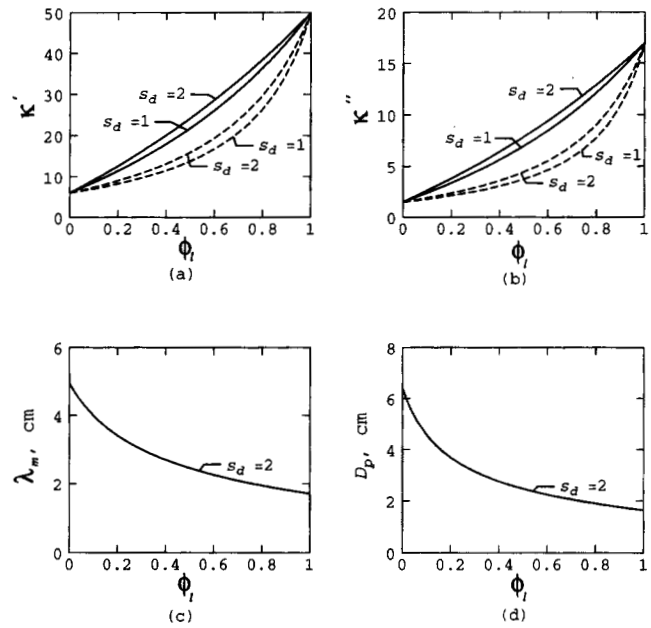

Figure 4. (a) Relative dielectric constant κ'; (b) relative dielectric loss κ''; (c) wavelength λ_{mi}; (d) penetration depth D_p of tylose as a function of liquid volume fraction, ϕ_l.

—— liquid continuous (LC) mushy zone; – – – solid continuous (SC) mushy zone.

are carried out for spherical dispersions $s_d = 2$. Both λ_m and D_p decrease with increasing ϕ_l as seen in Figure 4.

To check the validity of the finite-element solution of the effective heat capacity formulation, we have compared it with the analytical solution for the thawing of semi-infinite slab of ice (Carslaw and Jaeger, 1959). The analytical solution was obtained for a slab of pure ice with one end of the sample maintained at 300 K and the other end held at an initial temperature of 260 K. In order to use the effective heat capacity method to model the thawing of ice, we modified the liquid volume fraction vs. temperature curve for tylose so that the phase change occurred in a range of ± 0.5 K around the melting point of 273 K. This was achieved by setting the parameter values for T_i, T_m and T_f in Eq. 28 as 272.5 K, 273 K and 273.5 K, respectively.

The material properties used for ice are given in Table 1. A constant value of density 960 kg·m^{-3} was assumed for both the liquid and solid phases. To start the finite-element solution, a thin film of liquid is assumed to have formed. The thickness of this film corresponds to a thawing time of 1 s, and the temperatures within the liquid film were obtained from the analytical solution. The rest of the sample was kept at an initial temperature of 260 K, and temperatures were calculated for a sample of thickness 10 cm. Figure 5a compares the temperature in the liquid and solid regions obtained from numerical and analytical solutions. To avoid numerical errors due to the sharp change in the effective heat capacity at the melting point, we used about 40 quadratic elements in the first 1 cm of the sample. The computed temperatures are within 0.1% of the analytical solution. The slight discrepancy between the temperatures in the solid region during the first 10 s is due to the assumption of a uniform

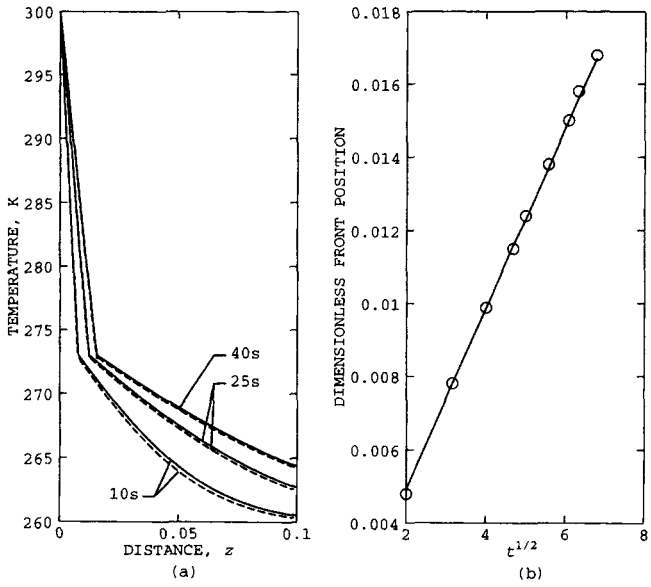

Figure 5. (a) Temperature distributions: —analytical and --- finite element solution; (b) front positions: — analytical solution and ○ finite element solution for ice predicted with a Dirichlet boundary condition.

2L = 10 cm, $I_{OL} \equiv I_{OR} = 0$.

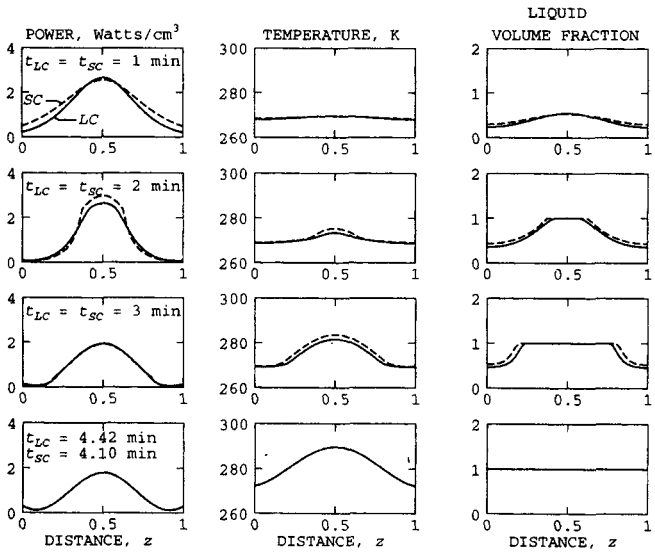

Figure 6. Power, temperature and liquid volume fraction profiles during microwave thawing of a 1-cm tylose slab exposed to microwaves.

f = 2,450 MHz, $I_{OL} \equiv I_{OR} = 3$ W·cm^{-2}. Thawing proceeds from the inside out, and differences between the solutions for the solid continuous and liquid continuous mushy zones is marginal.

initial temperature in the solid phase. The classical Stefan problem predicts a square root time dependence for the position of the melting front. Figure 5b illustrates the linear relationship between the dimensionless front position vs. $\sqrt{t}$ from our simulations.

Microwave thawing of tylose

Simulations were carried out for slabs of thickness varying between 1 to 5 cm. The heat-transfer coefficient h was chosen to be 2 W·m^{-2}·K^{-1}. Due to the lack of a good initial guess to begin the Newton scheme, a small time step $\Delta t = 1 \times 10^{-4}$ s was used at the first time step. Unless specified otherwise, $\Delta t = 0.1$ s was used for subsequent steps and typically 20–30 elements were used. Convergence tests were carried out with spatial and time refinements. It was found that the maximum difference for the values of the unknowns at the nodes was less than 1% when the values were compared for 20 and 40 elements. Similarly, the maximum difference was less than 1% when the results were compared for $\Delta t =$ 0.05 s and 0.1 s. All λ_m and D_p values reported are based on spatially averaged dielectric properties.

Figure 6 illustrates the spatial distribution of power, temperature and liquid volume fraction at various times for a sample of length 1 cm, exposed to microwaves of intensity 3 W·cm^{-2} from both faces. Initially, the sample is frozen and the magnitudes of λ_m and D_p are 5 and 6.4 cm respectively. Since the sample thickness is much smaller than D_p a peak in power absorption occurs at the center of the sample. As the temperature at each point in the sample reaches the initial melting point T_i, 265 K, the region turns mushy. At 1 min, it is observed that the temperatures in the sample are quite uniform and the entire sample is mushy ($0 < \phi_l < 1$). The liquid volume fraction ϕ_l is highest at the sample center due to the greater local power absorption. During the second minute, the center is fully thawed and the sample consists of a central liquid region surrounded by mushy zones. At 2 min, the power peak is still located at the sample center since the higher liquid volume fraction at the center increases the local effective dielectric loss. As a consequence, thawing occurs from the inside out. During the late stages of thawing ($t = 3$ min), D_p decreases to 1.64 cm, the power peak is still located at the center where the temperature is 280 K, and more than 50% of the sample is liquid. Thawing is completed at $t = 4.42$ min at which point the entire sample is liquid and $\phi_l = 1$ everywhere.

The dotted lines in Figure 6 show the results based on a solid continuous mushy zone. The results are both quantitatively and qualitatively very similar to that of the liquid continuous mushy zone. At $t = 1$ min, the spatially averaged value of D_p is 3.96 cm for the solid continuous case whereas it is 2.87 cm for the liquid continuous case. This is due to the lower dielectric loss for the solid continuous situation (Figure 4). Due to the increased penetration depth for the solid continuous model, the power absorption and consequently the temperature at the sample center is slightly higher resulting in a smaller thawing time of 4.10 min.

Results for thawing under identical conditions for a sample of length 2 cm are shown in Figure 7. After 1 min, the power, temperature and liquid volume fraction profiles look qualitatively similar to the profiles obtained for the 1 cm case. However, due to internal reflections the power absorbed at the faces of the 2 cm slab is low and the regions close to the sample boundaries remain frozen at the end of the first minute. At 2 min, a central liquid region is formed and power absorption at the outer surface of the sample increases. Due to the increase in power absorption at the outer faces, liquid

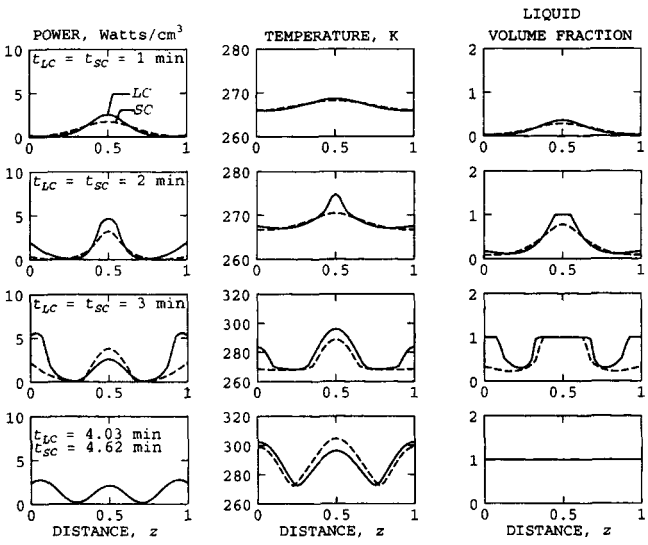

Figure 7. Power, temperature and liquid volume fraction profiles for a 2 cm tylose slab.

f = 2,450 MHz, $I_{OL} \equiv I_{OR}$ = 3 W·cm^{-2}. Thawing is seen to proceed from both the surface and within the sample.

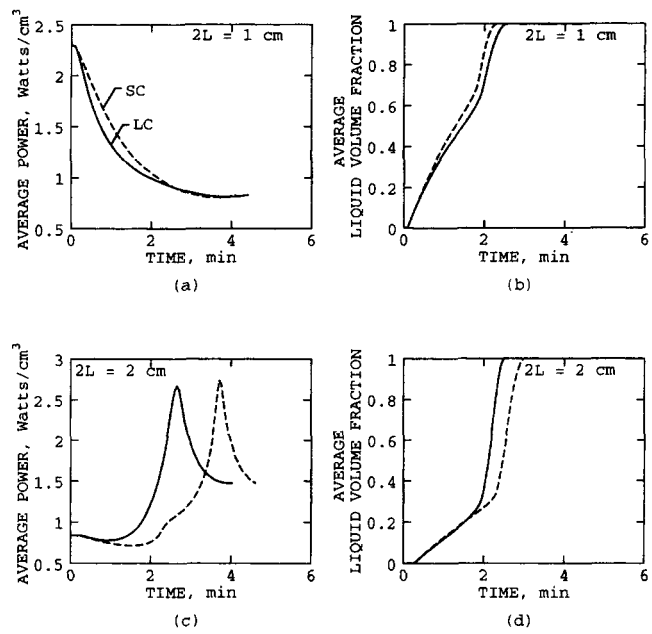

Figure 8. Average power and liquid volume fractions for 1-and 2-cm tylose slabs.

f = 2,450 MHz, $I_{OL} \equiv I_{OR}$ = 3 W·cm^{-2}. Resonance occurs for the 2 cm slab causing it to thaw quicker than the 1-cm slab.

regions are formed at the sample boundaries during the third minute. In contrast to the 1 cm sample, thawing proceeds both outwards from the center and inwards from the faces of the slab giving rise to four melting fronts. These multiple front situations which are captured using a fixed mesh illustrate the simplicity and advantage of the effective heat capacity method over the front tracking temperature based formulations. At t = 3 min, due to the increased dielectric loss in the outer liquid layer, the power deposited in the sample center decreases and the temperature in the outer regions increase. Contrast the final temperature profiles for the 2 cm sample with that of the 1 cm sample. Note that the 2 cm sample thaws in 4.03 min, whereas the 1 cm sample took 4.42 min under identical conditions.

Microwave thawing results are also shown for the solid continuous mushy zone. In this situation the differences in power absorption between the two models toward the later stages of thawing is quite significant. As a result, the thawing times for the solid continuous case is higher than the thawing times obtained for the liquid continuous case. Nevertheless, the differences in temperatures predicted between the two type of mushy zones though greater than the 1 cm sample are still small.

The anomalous decrease in thawing time for the 2 cm sample in comparison with the 1 cm sample can be explained by examining the average power and average liquid volume fraction as a function of time for both the 1 cm and 2 cm samples (Figure 8). Average values were obtained by integrating the quantity across the sample length and the average value of the liquid volume fraction was deduced from the ϕ_l vs. T relationship (Eq. 28 and Figure 3a) using a spatially averaged temperature. In the 1 cm sample, the average power is seen to decrease monotonically with time and the average value of the liquid volume fraction increases sharply around the second minute due to the formation of the inner liquid region (Figure 6). In contrast, the average power for the 2 cm sample is markedly different. Initially, the power absorbed is low; however, due to a resonant condition the power rises dramatically between the second and third minute (Figure 8c). The increase in power during the second minute can be attributed in part to the formation of outer liquid layers which increase the power absorption in the sample. The sharp rise in average power during the resonance leads to a rapid increase in thawing rate as seen in the average liquid volume fraction profile in Figure 8d, causing the 2 cm sample to thaw quicker than the 1 cm sample.

Resonances have been observed, by Barringer et al. (1994) during the microwave heating of cylindrical samples of water exposed to plane waves, and the conditions under which resonances occur in slabs and cylinders exposed to microwaves from one face have been investigated by Ayappa et al. (1996). Resonances in slabs exposed to microwaves from both faces were shown to occur when the slab thickness was an integral multiple of λ_m. These conditions for the occurrence of a resonance were derived for materials whose dielectric properties, and hence λ_m are constant throughout the sample. In situations where the wavelength is a function of the position in the sample, the standing wave patterns are more complex and resonances cannot be related in a simple manner to an average wavelength in the medium. Nevertheless, an average λ_m calculated at the resonant condition for the 2 cm slab is found to be 1.7 cm. It is interesting to note that the average power calculated assuming a solid continuous mushy region is qualitatively similar to that obtained for the liquid continuous model, however it is delayed.

Figure 9 illustrates the thawing phenomena for a sample of thickness 5 cm exposed to microwaves from both sides. During the initial stages, t = 1 min, λ_m is 3.96 cm, and the increased thickness leads to more node/antinode formations

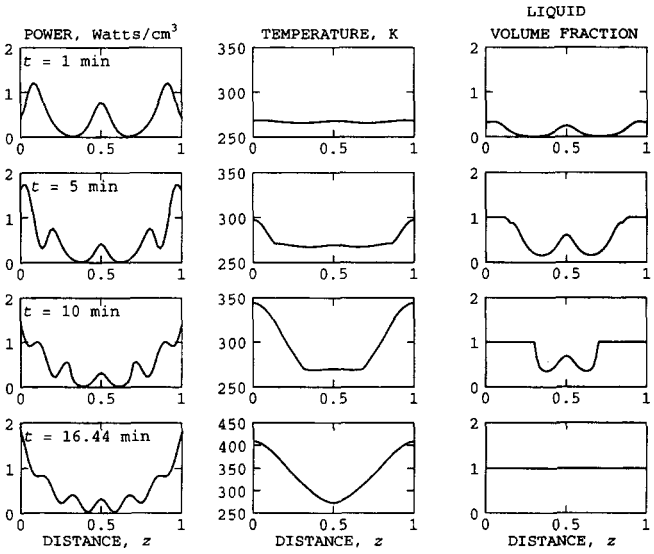

Figure 9. Power, temperature and liquid volume fractions for a 5-cm tylose slab.

$f = 2{,}450$ MHz, $I_{OL} \equiv I_{OR} = 3$ W·cm^{-2}. Thawing proceeds primarily from the surface of the slab leading to overheating of the liquid regions.

when compared with the thin samples. Maxima in the power occur both at the center and outer surfaces. During the first minute, the sample consists of three mushy regions separated by solid regions and the temperature is uniform across the sample. During the fifth minute, the outer regions have completely thawed and power is absorbed mostly at the sample boundaries. From the fifth to tenth minute, heating occurs primarily at the outer liquid layer and very little thawing takes place in the sample center. In contrast to the 1 and 2 cm samples, the sample center is the last to thaw and thawing proceeds from the outer faces of the slab. During the late stages, when the slab thickness is about 2.5 times D_p, the power profile decays into the sample following Lambert's law. When the slab is fully thawed at $t = 16.44$ min, it is observed that the outer surface temperature is around 400 K whereas the temperature at the center is 300 K. This overheating of liquid regions is a common problem encountered during microwave heating of thick samples. Although unrealistic for tylose, temperatures of 400 K can be attained in a microwave sterilization operation. Microwave power cycling is often used to avoid wasteful heating of the liquid regions and is examined in a later section.

Thawing is also examined for a 5 cm sample exposed to microwaves from one end as illustrated in Figure 10. Thawing occurs from the exposed side and at all times the sample consists of a liquid region at the exposed side followed by a mushy zone. As time progresses, the average penetration depth decreases to 2 cm and the power profile follows a Lambert's law behavior. Consequently, the temperature rise is very rapid near the exposed face, giving rise to hot spots and an uneven temperature profile within a sample. Due to the low microwave power absorption at the unexposed end, the temperature rise at this end is primarily due to heat being conducted from the exposed face.

Conventional thawing

We constrast the microwave thawing studies with conventional thawing. Figure 11 illustrates the thawing of a 1 cm slab of tylose in the absence of microwaves for a Dirichlet boundary condition of 300 K. Time steps range between 0.001–0.1 s. Qualitative features for thawing of the 1 cm and 5 cm (not shown) samples are similar. Thawing always originates from the outer surface, and the sample is characterized by a central mushy zone surrounded by liquid. Unlike mi-

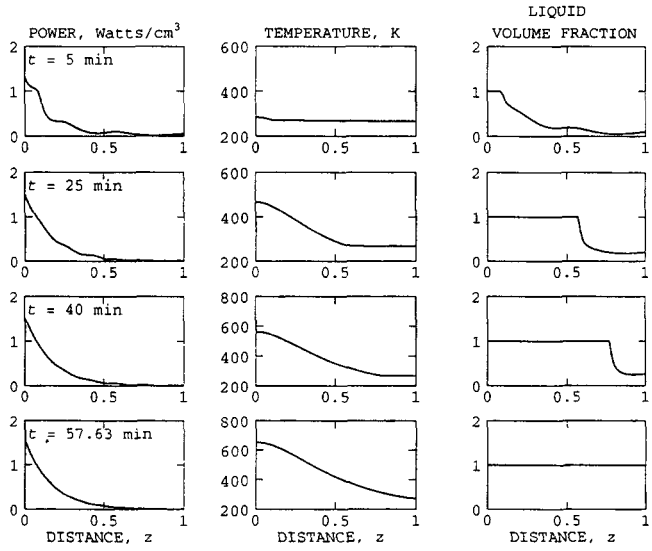

Figure 10. Power, temperature and liquid volume fractions for a 5-cm slab exposed to microwaves from the left face.

Thawing occurs from the exposed face only and heat is transferred by conduction to the far side. $f = 2{,}450$ MHz, $I_{OL} = 3$ W·cm^{-2}, $I_{OR} = 0$.

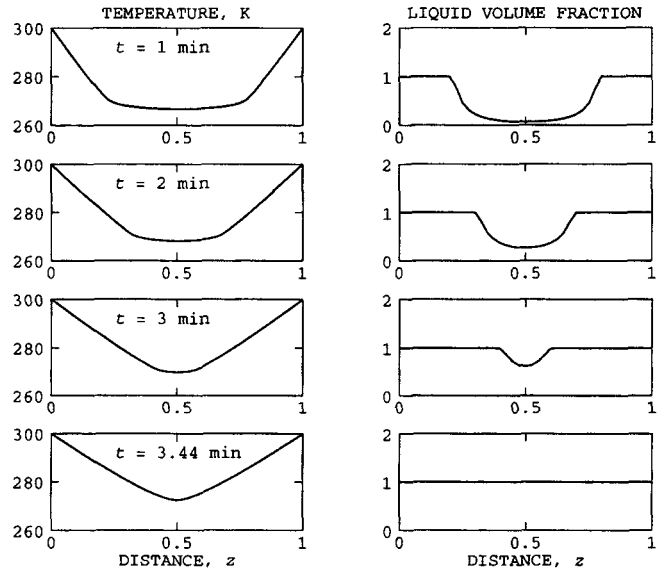

Figure 11. Temperature and liquid volume fraction distributions for 1 cm tylose slab with both ends at 300 K in the absence of microwaves.

Thawing occurs from outside.

crowave thawing, and consistent with the physical situation, multiple mushy regions were not observed during conventional thawing.

Thawing time vs. slab thickness

The correlation between thawing time t_{th} with slab thickness $2L$ for different situations are illustrated in Figure 12. For conventional thawing with a Dirichlet boundary condition of 300 K, the thawing time increases monotonically with sample thickness following a power law relationship $t_{th} \propto (2L)^n$. The exponent $n = 2$ is the classical Stefan problem result for thawing of a pure substance, where melting occurs at a distinct temperature and for materials that have a linear ϕ_l vs. T relationship (Carslaw and Jaeger, 1959). However, we observe a similar power law relationship for the ϕ_l vs. T curve of tylose for which no analytical results are available. This could probably be due to the small deviation from linearity in the ϕ_l vs. T relation for tylose. Deviations from linearity occur mainly during the initial and final stages of thawing (Figure 3). The exponent $n = 1.56$ for one face exposed to microwave radiation. When both faces of the sample were exposed to microwave radiation, a power law could not be used due to a resonance which reduced the thawing time for the 2 cm sample. In the study by Pangrle et al. (1992), the exponents for microwave thawing were 1.78 and 1.64 for beef and water, respectively. The larger exponent is due to the lower microwave power intensity of 0.5 $W \cdot cm^{-2}$ used in their calculations.

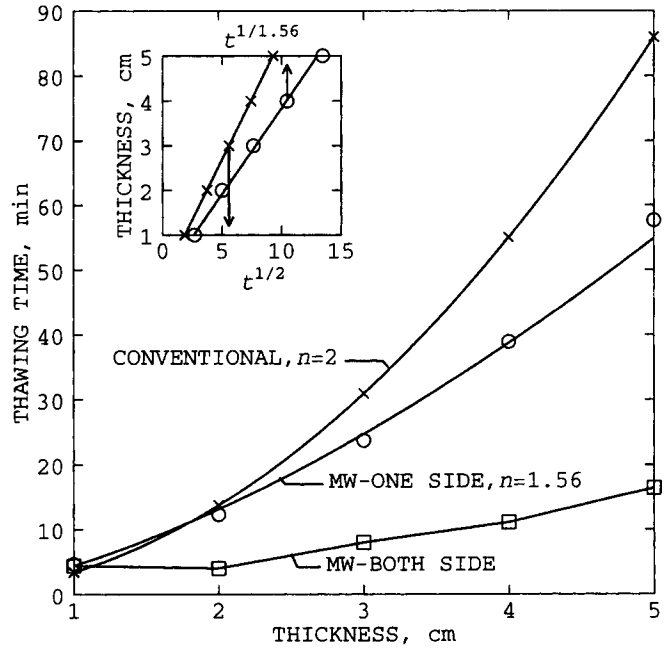

Figure 12. Thawing time vs. slab thickness is shown for conventional (Dirichlet boundary condition, 300 K) and microwave thawing.

For conventional thawing, the power law exponent $n = 2$ and for microwave thawing with one face exposed to microwaves, $n = 1.56$.

On-off control

As observed earlier (Figures 9 and 10), the overheating of liquid regions in thick samples during microwave heating leads to hot spots. This is a common problem encountered in both domestic and commercial applications. Domestic ovens attempt to overcome this problem by cycling the power with a simple on-off control with a fixed period. We simulated the on-off control on the microwave power as follows. The microwave power is switched off if the maximum temperature within the sample exceeds the upper bound of the setpoint, and it is switched on if the maximum temperature in the sample falls below the lower bound on the setpoint. The upper and lower temperature bounds are 5 degrees above and below the desired setpoint, respectively.

The on-off control is particularly advantageous for thick samples when the microwave source is of a high intensity. Figure 13 illustrates the results for a 5-cm slab with $I_{OL} \equiv I_{OR} = 10$ $W \cdot cm^{-2}$ as against 3 $W \cdot cm^{-2}$ used earlier (Figure 9) and a setpoint of 340 K. Due to the higher intensity of microwaves, time steps between 0.025–0.05 s had to be used for this case. At 5 min, although the extent of thawing is less, the temperature profile is more uniform with on-off control. During the final stages, the temperature rises unrealistically to 600 K in the absence of the on-off control. The total thawing time in the presence of control increases by about 2.5 times.

Figure 14 illustrates microwave power cycles for different setpoints in temperature. The results are shown for a 5 cm sample exposed to microwave intensity of 3 $W \cdot cm^{-2}$ on both sides. For a lower value of the setpoint, $T = 280$ K, the microwave source is off for most of the time. At $T = 300$ K, it is observed that initially the power is on for around 6 min, and cycling starts only after the sixth minute. For this case, the microwave power is on for about 1 min in each cycle. As the setpoint is increased, the duration for which the microwave power is on during the initial stages increases, the frequency

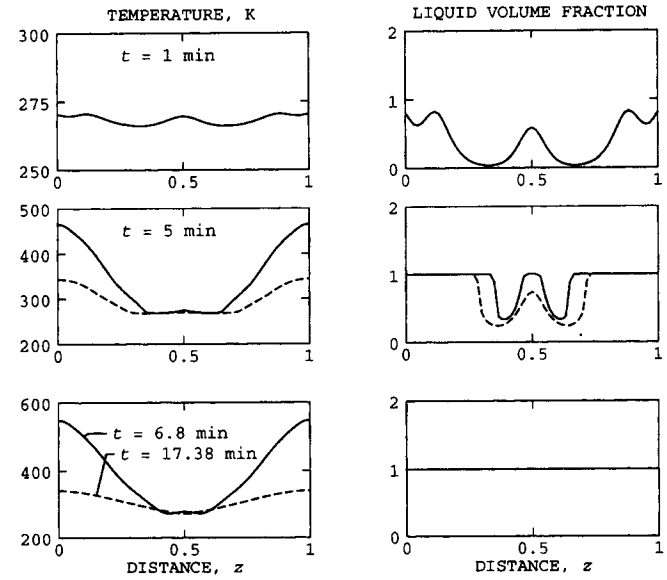

Figure 13. Temperature and liquid volume fraction distributions for a tylose slab exposed to microwaves with a setpoint of 340 K.

--- with on-off control; —— without on-off control. $2L = 5$ cm, $f = 2{,}450$ MHz, $I_{OL} \equiv I_{OR} = 10$ $W \cdot cm^{-2}$.

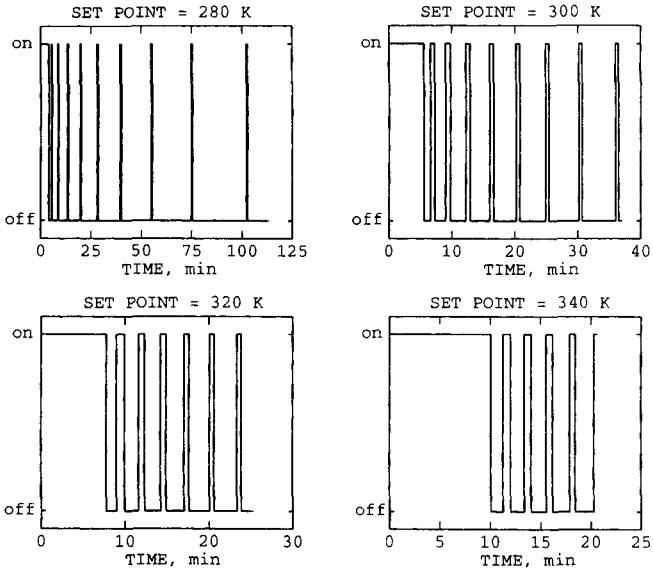

Figure 14. Power cycling for a 5-cm tylose slab for different setpoints.

As the setpoint is increased, thawing time decreases and the power consumption increases. $I_{OL} \equiv I_{OR} = 3\ \mathrm{W \cdot cm^{-2}}$.

of cycling decreases, and the power consumption increases. The thawing time decreases for higher values of the setpoint. For a setpoint of 340 K, the total thawing time is 20.60 min when compared with 16.44 min in the absence of any control (Figure 9) where the sample temperature exceeds 400 K.

Total thawing time and power savings as a function of the setpoint are illustrated in Figures 15a and 15b with $I_{OL} \equiv I_{OR} = 10\ \mathrm{W \cdot cm^{-2}}$. For all thicknesses, the thawing time decreases monotonically with an increasing setpoint (Figure 15a) with a more rapid decrease in thawing time for the thicker samples. As the setpoint is increased from 280 K to 340 K, the thawing time decreases from 6.6 min to 1.5 min, a factor of 4.4 for the 2 cm sample and 66 min to 9.3 min, and a factor of 7 for the 4 cm sample. In the thicker samples, thawing progresses with power being absorbed primarily in the outer liquid regions (Figure 9) while the interiors are heated by conduction. Since the temperatures in the inner regions which are the last to thaw are always below the lower bound (275 K) for the setpoint of 280 K, the temperatures in the liquid region control the microwave power cycling. In contrast, for thinner samples due to the increased penetration of microwaves, heating occurs more uniformly throughout the sample and the thawing time is less sensitive to an increase in the setpoint.

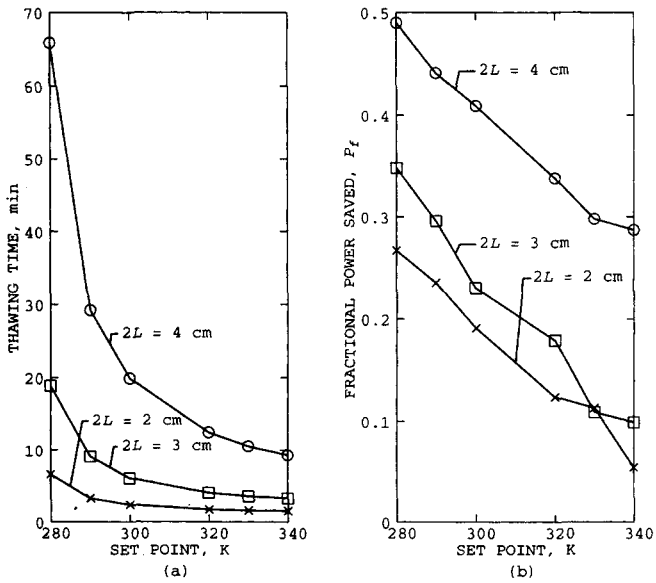

Figure 15. (a) Thawing time and (b) fractional power saved P_f (Eq. 29) vs. setpoint as a function of slab thickness.

$f = 2{,}450$ MHz, $I_{OL} \equiv I_{OR} = 10\ \mathrm{W \cdot cm^{-2}}$. Thawing time is a stronger function of the setpoint for the thicker samples and on-off control results in greater power saving for thicker slabs.

To investigate the extent to which power is saved with on-off control we define a quantity

$$P_f = 1 - \frac{\text{Time for power on with control}}{\text{Thawing time without control}}. \qquad (29)$$

$P_f = 0.5$ indicates that 50% of the power is saved by using cycling. Figure 15b illustrates the variation of P_f with the setpoint as a function of sample length. Power cycling results in greater power savings for thicker samples, where in the absence of control, power is used wastefully to heat liquid regions (Figure 9). However the decrease in P_f with the setpoint for all thicknesses is approximately the same.

Conclusion

We have modeled the microwave thawing of tylose slabs using the effective heat capacity formulation of the energy balance equation and Maxwell's equations for the microwave power. A single energy balance equation is used for the entire sample and the state of the material is determined from the equilibrium liquid volume fraction vs. temperature relationship for tylose.

Simulations for tylose slabs exposed to microwaves from both faces indicate that thawing can occur both from the center as well as the outside for thin samples. However for thick slabs exposed to microwaves from one face, thawing originates always from the surface. We observe a counterintuitive situation where a 2-cm slab thaws more quickly than a 1 cm slab due to the occurrence of a resonance. During a resonance, the increased power absorption results in higher thawing rates. Unlike materials with spatially independent dielectric properties, the highly nonlinear nature of the problem makes it difficult to derive length scales to predict these situations *a priori*. However, for samples greater than about 2.5 times the penetration depth, thawing is likely to progress from the outside.

We also contrast the use of effective dielectric properties of the mushy zone with both liquid continuous and solid continuous microstructures. Based on the premise that melting in solids is initiated at the grain boundaries, we feel that a liquid continuous mushy zone is a more appropriate characterization for the mushy zone.

The thawing time varies with sample length following a power law. The exponent is 2 for conventional thawing and

1.56 when the slab is exposed to microwaves from one end. In the case of microwave thawing, the exponent is dependent on the intensity of the incident microwaves. The power law could not be applied for samples exposed to microwaves on both sides due to the resonance in the 2-cm sample. On-off control was implemented to prevent excessive heating of the liquid regions. Studies show that the power saved is greater for thick samples.

Although the method is illustrated for tylose, the model can be used to study microwave thawing of other materials that melt over a temperature range. The most common situation is perhaps the thawing of frozen foods where a better understanding of the dynamics of microwave thawing can lead to improved product design. In addition of being more appropriate than the temperature formulations for materials that melt over a range of temperatures, the effective heat capacity method uses a fixed mesh. This can be particularly advantageous when dealing with 2-D and 3-D models. We are currently investigating these situations.

Acknowledgment

We thank the Supercomputer Education and Research Center, Indian Institute of Science, for computing resources and Dr. T. A. Abinandanan and Dr. J. Srinivasan for useful discussions on the mushy zone.

Literature Cited

Ayappa, K. G., H. T. Davis, E. A. Davis, and J. Gordon, "Analysis of Microwave Heating of Materials with Temperature-Dependent Properties," *AIChE J.*, **37**, 313 (1991).

Ayappa, K. G., H. T. Davis, E. A. Davis, and J. Gordon, "Two-Dimensional Finite Element Analysis of Microwave Heating," *AIChE J.*, **38**, 1577 (1992).

Ayappa, K. G., H. T. Davis, S. A. Barringer, and E. A. Davis, "Resonant Heating in Slabs and Cylinders Exposed to Plane Waves," **43**, 615, 7 (1997).

Barringer, S. A., E. A. Davis, J. Gordon, K. G. Ayappa and H. T. Davis, "The Effect of Sample Size on Microwave Heating Rate: Comparison of Oil and Water," *AIChE J.*, **40**, 1433 (1994).

Carslaw, H. S., and J. C. Jaeger, *Conduction of Heat in Solids*, Oxford at Clarendon Press (1959).

Chan, A. K., R. A. Sigelmann, A. W. Guy, and J. F. Lehmann, "Calculation by Method of Finite Difference of the Temperature Distribution in Layered Tissues," *IEEE Trans. Biomed. Eng.*, **20**, 86 (1973).

Coleman, C. J., "The Microwave Heating of Frozen Substances," *Appl. Math. Modelling*, **14**, 439 (1990).

Dalhuijsen, A. J., and A. Segal, "Comparison of Finite Element Techniques for Solidification Problems," *Int. J. Num. Methods in Eng.*, **23**, 1807 (1986).

Dantzig, J. A., "Modelling Liquid-Solid Phase Changes with Melt Convection," *Int. J. Num. Methods in Eng.*, **28**, 1769 (1989).

Datta, A. K., "Heat and Mass Transfer in the Microwave Processing of Food," *Chem. Eng. Prog.*, **6**, 47 (1990).

De Wagter, C., "Computer Simulation Predicting Temperature Distributions Generated by Microwave Absorption in Multilayered Media," *J. Microwave Power*, **19**, 97 (1984).

Fricke, H., "The Complex Conductivity of a Suspension of Stratified Particles of Spherical or Cylindrical Form," *J. Phy. Chem.*, **56**, 168 (1955).

Hill, J. M., and T. R. Marchant, "Modelling Microwave Heating," *Appl. Math. Modelling*, **20**, (1996).

Jolly, P., and I. Turner, "Non-Linear Field Solutions of One-Dimensional Microwave Heating," *J. Microwave Power and EM Energy*, **25**, 3 (1990).

Pangrle, B. P., K. G. Ayappa, H. T. Davis, E. A. Davis and J. Gordon, "Microwave Thawing of Cylinders," *AIChE J.*, **37**, 1789 (1991).

Pangrle, B. P., K. G. Ayappa, E. Sutanto, H. T. Davis, E. A. Davis, and J. Gordon, "Microwave Thawing of Lossy Dielectric Materials," *Chem. Eng. Comm.*, **112**, 39 (1992).

Taoukis, P., E. A. Davis, H. T. Davis, J. Gordon, and Y. Talmon, "Mathematical Modeling of Microwave Thawing by the Modified Isotherm Migration Method," *J. Food Sci.*, **52**, 455 (1987).

Voller, V. R., C. R. Swaminathan, and B. G. Thomas, "Fixed Grid Techniques for Phase Change Problems: A Review," *Int. J. Num. Methods in Eng.*, **30**, 875 (1990).

Zeng, X., and A. Faghri, "Experimental and Numerical Study of Microwave Thawing Heat Transfer of Food Materials," *ASME Trans. J. Heat Transfer*, **116**, 446 (1994).

Appendix

Electromagnetic waves are composed of electric ($\boldsymbol{E}$) and the magnetic fields ($\boldsymbol{H}$). The governing equations for a propagating electromagnetic wave are represented by Maxwell's equations, which in differential form are

$$\nabla \times \boldsymbol{E} = -\frac{\partial \boldsymbol{B}}{\partial t}, \tag{A1}$$

$$\nabla \times \boldsymbol{H} = \boldsymbol{J} + \frac{\partial \boldsymbol{D}}{\partial t}, \tag{A2}$$

$$\nabla \cdot \boldsymbol{D} = \rho, \tag{A3}$$

and

$$\nabla \cdot \boldsymbol{B} = 0. \tag{A4}$$

where $\boldsymbol{E}$ is the electric field, $\boldsymbol{H}$ the magnetic field, $\boldsymbol{J}$ the current flux, $\boldsymbol{D}$ the electric displacement, ρ the electric charge density, and $\boldsymbol{B}$ the magnetic induction. The constitutive equations relating $\boldsymbol{J}$, $\boldsymbol{D}$, and $\boldsymbol{B}$ to $\boldsymbol{E}$ and $\boldsymbol{H}$ are

$$\boldsymbol{J} = \sigma(\omega)\boldsymbol{E}(t),\ \boldsymbol{D} = \epsilon(\omega)\boldsymbol{E}(t) \quad \text{and} \quad \boldsymbol{B} = \mu(\omega)\boldsymbol{H}(t), \tag{A5}$$

where $\sigma(\omega)$ is the electrical conductivity, $\epsilon(\omega)$ is the permittivity, $\mu(\omega)$ is the magnetic permeability of the material, and $\omega = 2\pi f$, where f is the frequency of electromagnetic radiation. We consider linear dielectric materials where $\sigma(\omega)$, $\epsilon(\omega)$ and $\mu(\omega)$ are independent of field intensities. However, $\sigma(\omega)$, $\epsilon(\omega)$ and $\mu(\omega)$ are in general functions of the temperature within the sample.

Assuming a time dependence of the form $e^{-i\omega t}$, the instantaneous field vectors can be represented as

$$\boldsymbol{E}(\boldsymbol{r}, t) = \bar{\boldsymbol{E}}(\boldsymbol{r})e^{-i\omega t} \quad \text{and} \quad \boldsymbol{H}(\boldsymbol{r}, t) = \bar{\boldsymbol{H}}(\boldsymbol{r})e^{-i\omega t}. \tag{A6}$$

Substituting the constitutive relations for $\boldsymbol{J}$ and $\boldsymbol{D}$ from Eqs. A5 and field relations from Eqs. A6 into Eq. A2 we get

$$\nabla \times \bar{\boldsymbol{H}} = -i\omega\epsilon^*(\omega)\bar{\boldsymbol{E}} + \frac{\partial \epsilon}{\partial \phi_l}\frac{d\phi_l}{dT}\frac{\partial T}{\partial t}\bar{\boldsymbol{E}}, \tag{A7}$$

where

$$\epsilon^*(\omega) = \epsilon'(\omega) + i\epsilon''(\omega)$$

and $\epsilon' = Re(\epsilon^*)$ and $\epsilon'' = Im(\epsilon^*)$. The last term of Eq. A7 is due to the dependence of ϵ on the liquid volume fraction (ϕ_l) which is in turn a function of temperature. To simplify the notation, the overbar on $\bar{E}$ and $\bar{H}$ will be dropped from this point on. If the time scales for electromagnetic propagation are significantly smaller than that for thermal transport, the last term can be neglected. This is easily seen if Eq. A7 is put in dimensionless form.

Using

$$H' = \frac{H}{H_0},\ E' = \frac{E}{E_0},\quad \theta = \frac{T}{T_0},\ \nabla' = L\nabla \text{ and } \tau = \frac{\alpha_T t}{L^2} \tag{A8}$$

with

$$\frac{E_0}{H_0} = \sqrt{\mu_0/\epsilon_0},\ c = \frac{1}{\sqrt{\epsilon_0 \mu_0}} \quad \text{and} \quad \lambda_0 = \frac{c}{f}, \tag{A9}$$

Eq. A7 can be written as

$$\frac{\lambda_0}{2\pi L}\nabla' \times H' = -i\kappa^* E' + \frac{\alpha_T}{L^2\omega}\frac{\partial \kappa}{\partial \phi_l}\frac{d\phi_l}{d\theta}\frac{\partial \theta}{\partial \tau}E'. \tag{A10}$$

In Eqs. A8 and A9, E_0, H_0 and T_0 are reference quantities, L is a characteristic sample dimension and α_T is the thermal diffusivity in the sample. The dimensionless group

$$\frac{\alpha_T}{L^2\omega} = \frac{1/\omega}{L^2/\alpha_T}, \tag{A11}$$

represents the ratio of the time scale for electromagnetic propagation to that of thermal diffusion. For the gigahertz frequencies and typical sample dimensions used in microwave thawing applications, it turns out that the order of magnitude of the dimensionless group in Eq. A11 is $O(10^{-14})$.

In the mushy region, the effective dielectric constant κ is a continuous function of ϕ_l. However, the ϕ_l vs. T relationship generally has discontinuities at $\phi_l = 0$ and $\phi_l = 1$. To avoid numerical difficulties while using the effective heat capacity method, these discontinuous regions in the ϕ_l vs. T relationship are replaced by continuously differentiable functions. In these situations Eq. A7 reduces to

$$\nabla \times H = -i\omega\epsilon^*(\omega)E. \tag{A12}$$

If the magnetic permeability within the sample is that of free space μ_0 then Eq. A1 is

$$\nabla \times E = i\omega\mu_0 H. \tag{A13}$$

In deriving Eq. A13 we have used the field relations from Eq. A6. The differential equation for the electric field in a nonhomogeneous medium can be derived from Eqs. A12, A13 and $\nabla\cdot(\epsilon^* E) = 0$, which is obtained by taking the divergence of Eq. A12. Taking the curl of Eq. A13 and using the identities $\nabla \times (\nabla \times E) = \nabla(\nabla\cdot E) - \nabla^2 E$ and $\nabla\cdot(\kappa^* E) = \kappa^*\nabla\cdot E + \nabla\kappa^*\cdot E$, the magnetic field can be eliminated from Eq. A13 resulting in the differential equation for the electric field within the sample

$$\nabla\left(E\cdot\frac{\nabla\kappa^*}{\kappa^*}\right) + \nabla^2 E + k(T)^2 E = 0, \tag{A14}$$

where $\kappa^* = \epsilon^*/\epsilon_0$. The first term in Eq. A14 is zero for a sample exposed to plane waves and Eq. A14 reduces to

$$\nabla^2 E + k(T)^2 E = 0. \tag{A15}$$

The 1-D form of Eq. A15 is Eq. 9 in this article.

Manuscript received July 15, 1996, and revision received Jan. 15, 1997.